Multisite Structure of $PbWO_4:Eu^{3+}$ Crystals Investigated by Site-Selective Laser-Excitation Spectroscopy

Yanlin Huang[†] and Hyo Jin Seo*[,‡]

College of Chemistry, Chemical Engineering and Materials Science, Soochow University, Suzhou 215123, China, and Department of Physics, Pukyong National University, Busan 608-737, Korea

Received: February 6, 2009; Revised Manuscript Received: March 7, 2009

Defect structures of Eu^{3+}-doped $PbWO_4$ crystals are investigated by site-selective laser-excitation spectroscopy. The excitation spectrum of the $^7F_0 \rightarrow {}^5D_0$ transition shows a strong dependence on Eu^{3+}-concentration in $PbWO_4$ crystals. Only one substitution site for Eu^{3+} is identified in the $PbWO_4:Eu^{3+}$ (0.01 at.%) crystal, while at least six inequivalent sites are observed in the $PbWO_4:Eu^{3+}$ (0.05 and 0.5 at.%) crystals. The charge compensation mechanisms for the observed sites are discussed in relation with annealing effects and temperature-dependent decay curves. The dominant site for Eu^{3+} in the $PbWO_4$ lattice seems to be due to a formation of $Eu_{Pb}^{3+}-V_{Pb}''$ dipole by charge compensation. The minor sites for Eu^{3+} are attributable to the $Eu_{Pb}^{3+}-O_i''$ dipole, a site perturbed by $Eu_{Pb}^{3+\bullet}-V_{Pb}''$ dipole, and a clustering of Eu^{3+} in the $PbWO_4$ lattice. The energy transfer and site distribution of Eu^{3+} are discussed in $PbWO_4:Eu^{3+}$ (0.01, 0.05, and 0.5 at.%).

I. Introduction

The $PbWO_4$ crystal is one of the well-known scintillation materials. Doping of the $PbWO_4$ crystal by trivalent rare earth ions (RE^{3+}) improves its scintillation properties[1−3] and has been performed for the purpose of other applications, for example, promising laser host crystals,[4,5] Cherenkov crystals,[6] and high-temperature ionic conductors.[7] The $PbWO_4$ crystal has a typical Scheelite-type structure ($I4_1/a$) to accommodate a large concentration of RE^{3+} ions.[2] When Eu^{3+} is incorporated in the $PbWO_4$ lattice, on a regular lattice, it must be accompanied by a charge-compensating defect. Much attention has therefore been paid to investigate defect structure of $PbWO_4:RE^{3+}$.[8,9] Some of the RE^{3+}-doping mechanism is not clear because of the structure-sensitive properties of $PbWO_4$. In the case of doping by RE^{3+} with high concentration in $PbWO_4$, the defect structure becomes more complex because of a variety of charge-compensation processes in the crystal lattice. Among the suggested defect structures, some of them were calculated on the basis of different hypotheses and were not directly confirmed by luminescence experiments.

A change in local structure because of the substitution of RE^{3+} for the host cation in a crystal lattice is not easy to characterize by using X-ray diffraction (XRD) because XRD is mainly sensitive to the host cation ions. Luminescence measurements would give much information about the local surroundings of RE^{3+} in the host lattice. Oxygen is one of the important factors for the defect structure in the $PbWO_4$ lattice.[10−13] The oxygen sublattice is almost invisible in XRD in compounds.

We use site-selective laser-excitation spectroscopy to investigate substitution sites for Eu^{3+} and defect structures of the Eu-doped $PbWO_4$ crystals. The narrow excitation and emission lines due to the $4f \rightarrow 4f$ transitions of Eu^{3+} in $PbWO_4$ offer a convenient method for directly monitoring the different sites. Eu^{3+} has a simple multiplet pattern of its energy level which makes this ion particularly suited as a probe of local structure.[14,15] Recently, luminescent properties have been investigated in RE^{3+}-doped $PbWO_4$:crystals.[16−19] However, no defect structure has been investigated in detail in RE-doped $PbWO_4$ crystals, and luminescent properties concerning Eu^{3+} have been rarely reported in $PbWO_4$. In this study, we present in detail the luminescent properties and multisite structures of Eu^{3+} in $PbWO_4$.

II. Experimental Section

Single crystals of $PbWO_4$ doped with Eu^{3+} ions were grown from the melt by the Czochralski method. The concentrations of Eu^{3+} were 0.01, 0.05, and 0.5 at.% in the melt. The excitation source was a dye laser (Spectron Laser Sys. SL4000) pumped by the second harmonic (532 nm) of a pulsed Nd:YAG (yttrium aluminum garnet) laser (Spectron Laser Sys. SL802G). The laser beam was focused inside the sample with a cross-sectional area of about 3 mm^2. The pulse energy was about 5 mJ with 10 Hz repetition rate and 5 ns duration. The samples were placed in a helium gas flow cryostat for measurements in the variable-temperature region (10−300 K). The luminescence was dispersed by a 75 cm monochromator (Acton Research Corp. Pro-750) and was observed with a photomultiplier tube (PMT) (Hamamatsu R928). The signal from PMT was fed into a digital oscilloscope (LeCroy 9350A) with which emission and excitation spectra and decay curves were obtained. The excitation spectra for the $^7F_0 \rightarrow {}^7D_0$ transition were obtained by monitoring the total luminescence (wavelengths > 585 nm) detecting with the monochromator in zero order of diffraction. Suitable filters were used to eliminate the intense scattering peaks in the spectrum because of the scattered laser irradiation. The slit widths of the monochromator were normally set to give a resolution of 0.025 nm for emission spectra. Annealing experiments were taken on the sample at oxygen atmosphere. The samples were heated up to the designed temperature, were kept at this temperature for 8 h, and then were quenched down to room temperature by letting them cool down in the platinum boat in which they were heated.

* To whom correspondence should be addressed. E-mail: hjseo@pknu.ac.kr.
[†] Soochow University.
[‡] Pukyong National University.

10.1021/jp901099h CCC: $40.75
Published on Web 04/09/2009

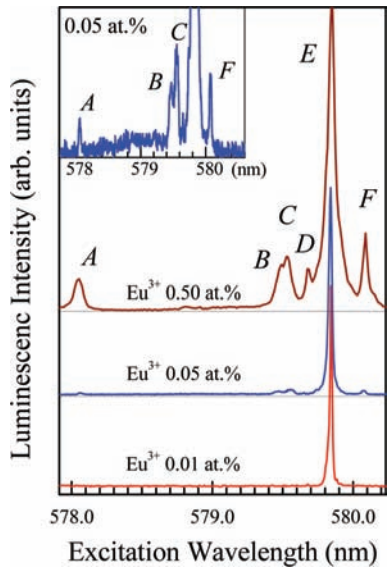

Figure 1. Excitation spectra of the $^7F_0 \rightarrow {}^5D_0$ transition obtained by monitoring the emissions due to the $^5D_0 \rightarrow {}^7F_J$ (J = 1, 2, 3,..., 6) transitions in $PbWO_4$:Eu^{3+} (0.01, 0.05, and 0.5 at.%) at 10 K. The peaks in $PbWO_4$:Eu^{3+} (0.5 at.%) are labeled by A, B, C, D, E, and F. The inset is the enlarged excitation spectrum of $PbWO_4$:Eu^{3+} (0.05 at.%).

III. Results and Discussion

1. Excitation Spectra of the $^7F_0 \rightarrow {}^5D_0$ Transition. Figure 1 shows the $^7F_0 \rightarrow {}^5D_0$ excitation spectra of $PbWO_4$:Eu^{3+} (0.01, 0.05, and 0.5 at.%) obtained by monitoring the luminescence (wavelengths > 585 nm) due to the $^5D_0 \rightarrow {}^7F_J$ (J = 1, 2,..., 6) transitions at 10 K. We observe the most intense line at 579.85 nm for three samples. The spectrum of $PbWO_4$:Eu^{3+} (0.5 at.%) consists of six lines, that is, the intense line at 579.85 nm (labeled by E) and the five weak lines labeled by A (578.06 nm), B (579.50 nm), C (579.55 nm), D (579.69 nm), and F (580.08 nm) as indicated in Figure 1. In $PbWO_4$:Eu^{3+} (0.01 at.%), the weak excitation lines were not detected in the temperature region of 10−300 K. The extended excitation spectrum of $PbWO_4$:Eu^{3+} (0.05 at.%) (see inset of Figure 1) exhibits five weak lines which are observed at the same wavelengths in the spectrum of $PbWO_4$:Eu^{3+} (0.5 at.%).

The Pb^{2+} for Eu^{3+} has S_4 crystal field symmetry in $PbWO_4$ structure.[20] According to the symmetry selection rules, the $^7F_0 \rightarrow {}^5D_0$ transition is strictly forbidden for the S_4 symmetry.[21] The presence of excitation lines because of the $^7F_0 \rightarrow {}^5D_0$ transition indicates that Eu^{3+} in $PbWO_4$ experiences crystal field symmetry lower than S_4. The lower crystal field symmetry on Eu^{3+} is due to the charge compensation or to intrinsic structural defects, such as structural vacancy (Pb or O) and interstitial oxygen in the $PbWO_4$ lattice. All the excitation lines are getting broader by increasing Eu^{3+} concentration. A large structural disorder in the environment around Eu^{3+} is responsible for the broadening of lines.

Each line appearing in the excitation spectra of the $^7F_0 \rightarrow {}^5D_0$ transition corresponds to a different Eu^{3+} center since the transition between the nondegenerate $^7F_0$ and $^5D_0$ levels can have only one line per site. This means that the Eu^{3+} ions occupy at least six different sites in $PbWO_4$:Eu^{3+} (0.05 and 0.5 at.%) and only one detectable site in $PbWO_4$:Eu^{3+} (0.01 at.%). Hereafter, we call the sites giving rise to the six excitation the sites Eu^{3+}(A), Eu^{3+}(B), Eu^{3+}(C), Eu^{3+}(D), Eu^{3+}(E), and Eu^{3+}(F).

2. Selectively Excited Emission Spectra. Figure 2 shows the $^5D_0 \rightarrow {}^7F_J$ (J = 1−4) emission spectrum of $PbWO_4$:Eu^{3+} (0.01 at.%) under the excitation at 579.85 nm (site E) at 10 K. Nearly the same spectral features were observed for $PbWO_4$:Eu^{3+} (0.05 and 0.5 at.%). As shown in Figure 2, the $^7F_1$ multiplet splits completely into three levels indicating that Eu^{3+} substitutes for a site with lower crystal field symmetry than cubic, hexagonal, and tetragonal symmetries.[21] Figure 3 shows the emission spectra of $PbWO_4$:Eu^{3+} (0.5 at.%) obtained by tuning the laser to resonance with each excitation line of A−F at 10 K. The emission spectra could be discerned into three groups, that is, F and B; A; and C, D, and E in which each group has similar spectral features. The appearance of more than four emission lines of the $^5D_0 \rightarrow {}^7F_1$ transition for the sites F, B, and A is due to the spectral overlap of other sites. The energy levels of the $^5D_0$ and ^7F_J (J = 1−4) multiplets of Eu^{3+} at each site were determined from the emission and excitation spectra at low temperature (listed in Table 1). The emissions due to the $^5D_0 \rightarrow {}^7F_J$ (J = 5 and 6) transitions were too weak to be detected.

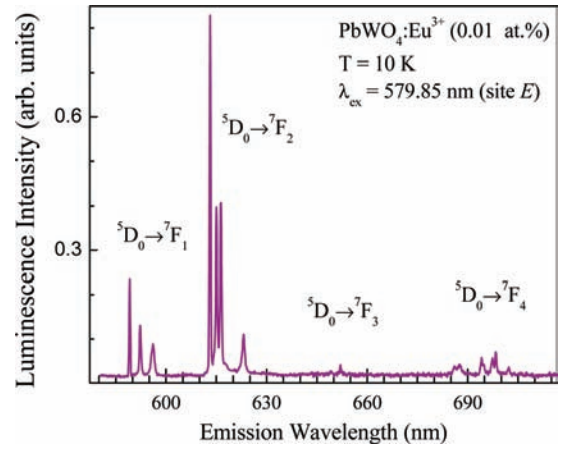

Figure 2. The emission spectrum of the $^5D_0 \rightarrow {}^7F_J$ (J = 0−4) transitions under the excitation at 579.85 nm (site E) at 10 K in $PbWO_4$:Eu^{3+} (0.01 at.%).

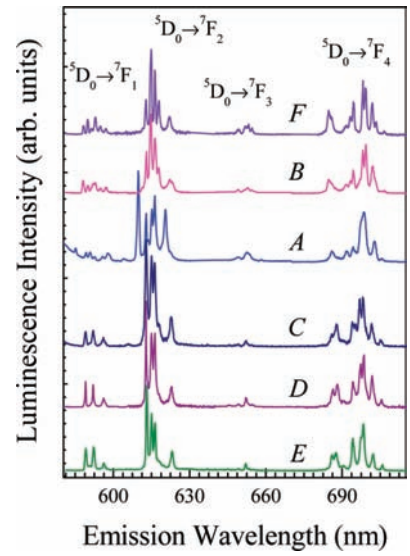

Figure 3. The $^5D_0 \rightarrow {}^7F_J$ (J = 0−4) emission spectra obtained by the excitation of sites A (578.06 nm), B (579.50 nm), C (579.55 nm), D (579.69 nm), E (579.85 nm), and F (580.08 nm) at 10 K in $PbWO_4$:Eu^{3+} (0.5 at.%). Intensities are normalized to the most intense $^5D_0 \rightarrow {}^7F_2$ peak.

3. Temperature Dependence of Transient Behavior of the Luminescence. Decay curves of the $^5D_0$ emission were obtained by exciting the Eu^{3+} ions at each site in the three samples in

TABLE 1: Estimated Energy Levels of Eu^{3+} for Sites A−F in $PbWO_4$ Obtained from Excitation and Emission Spectra at 10 K

	A[a]	B	C	D	E	F
$^7F_0$	0	0	0	0	0	0
$^7F_1$	210	254	261	276	272.9	236
	310	306	359	362	359	286
	421	378		478	476	372
	516	441				423
		507	506			492
$^7F_2$	915	943	913	937	936	921
	988	9823	947	990	988	964
	1045	1030	983	1026	1022	1016
	1050	1069	1023	1202	1198	1055
	1191	1186	1056			1164
	1249		1201			
			1207			
$^7F_3$	1890	1846	1851	1769	1791	1760
	1905	1916	1913	1853	1847	1822
	1973	1944	1936	1917	1913	1839
	2003	1977	1981	1975	1935	1897
	2103	1994			1978	1908
						1930
						1960
$^7F_4$	2721	2654	2684	1975	2670	2628
	2842	2684	2802	2666	2703	2778
	2898	2798	2844	2714	2841	2806
	2963	2834	2908	2842	2908	2837
	2987	2854	2930	2868	2929	2911
	3073	2932	2959	2901	3004	2934
	3128	2957	3000	2928	3078	2986
		3012	3019	2986		3018
		3099	3076	3071		3082
$^5D_0$	17299	17256	17255	17251	17246	17239

[a] Units in cm^{-1}.

the temperature region of 10−300 K. The decay curves (Figures 4 and 5a) represent strong dependence on Eu^{3+} concentration and sample temperature. Temperature-dependent decay behavior of Eu^{3+}(E) in $PbWO_4:Eu^{3+}$ (0.01 and 0.05 at.%) (Figure 4a) is significantly different from that in $PbWO_4:Eu^{3+}$ (0.5 at.%) (Figure 5a). The luminescence decay curves are single exponential for $PbWO_4:Eu^{3+}$ (0.01 and 0.05 at.%) (Figure 4a), while the decays are nonexponential for $PbWO_4:Eu^{3+}$ (0.5 at.%) (Figure 5a) in the temperature region of 10−300 K.

Figure 4b shows the lifetime values of the $^5D_0$ emission of Eu^{3+}(E) as a function of temperature in $PbWO_4:Eu^{3+}$ (0.01 and 0.05 at.%). Temperature dependence of the decay times in Figure 4b is a typical thermal quenching process. The decay time maintains nearly the same value of about 0.51 ms in the temperature range of 10−175 K, and then quenching occurs at temperatures higher than 175 K. In the thermal quenching process, energy transfer occurs from Eu^{3+} to killer centers or to any other defect centers near the Eu^{3+} ions by thermal phonon assistance. One cannot expect that the quenching is due to the multiphonon relaxation from the $^5D_0$ level to the ^7F_J levels because of the large energy gap (>10 000 cm^{-1}) between the $^5D_0$ and $^7F_6$ levels. The quenching process is described by the form

$$\tau_{exp}^{-1} = \tau_0^{-1} + Ke^{-\Delta E/kT} \quad (1)$$

where τ_0 is the intrinsic lifetime of the $^5D_0$ level, K is the nonradiative rate factor (i.e., nonradiative rate in the condition of $\Delta E = 0$), and ΔE is the activation energy of nonradiative recombination.[22,23] The best fit, shown by the solid line in Figure 4b, describes the main feature of the temperature dependence. The resulting best fit parameters are given in Figure 4b.

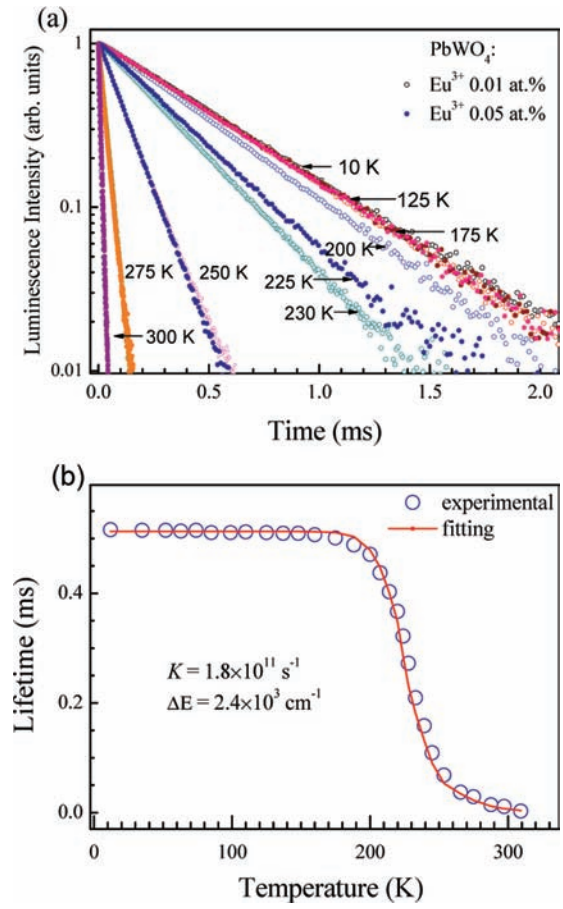

Figure 4. (a) Luminescence decay curves of the $^5D_0$ level for site E (579.85 nm) in the $PbWO_4:Eu^{3+}$ (0.01 and 0.05 at.%) crystals at various temperatures. Open circles represent decay curves for $PbWO_4:Eu^{3+}$ (0.01 at.%) and closed circles for $PbWO_4:Eu^{3+}$ (0.05 at.%). (b) Decay times of the $^5D_0$ level as a function of temperature obtained by fitting the decay curves on the basis of single exponential. The continuous line is the fitting to the theoretical model given by eq 1.

The nonexponential decay curves (Figure 5a) for $PbWO_4:Eu^{3+}$ (0.5 at.%) are well fitted to the energy-transfer model suggested by Inokuti and Hirayama[24−26] in the temperature region of 10−175 K. The energy-transfer process for the dipole−dipole interaction between two Eu^{3+} ions is given by the equation

$$I(t) = \exp\left[-\frac{t}{\tau_0} - \frac{n}{n_0}\sqrt{\pi}\left(\frac{t}{\tau_0}\right)^{1/2}\right] \quad (2)$$

where n is the concentration of Eu^{3+} ions, that is, the number per unit volume, and n_0 is the critical concentration defined in terms of a critical transfer distance R_0 (T) between two Eu^{3+} ions at temperature T, that is, $n_0 = ((4/3)\pi R_0^3)^{-1}$. The energy-transfer rate W_{ET} (R_A) between two Eu^{3+} ions with an average distance R_A by dipole−dipole interaction can be written by

$$W_{ET}(R_A) = \tau_0^{-1}\left(\frac{R_0(T)}{R_A}\right)^6 \quad (3)$$

The energy-transfer rate W_{ET} (R_A) is calculated by eq 3 with the parameters obtained by fitting the decays from eq 2.

The fitting of decay, however, begins to deviate from eq 2 at temperatures higher than 175 K and could not fit above 250 K by this energy-transfer model. It seems that the energy diffusion among the Eu^{3+} ions together with the thermal quenching processes is responsible for the deviation at higher temperatures

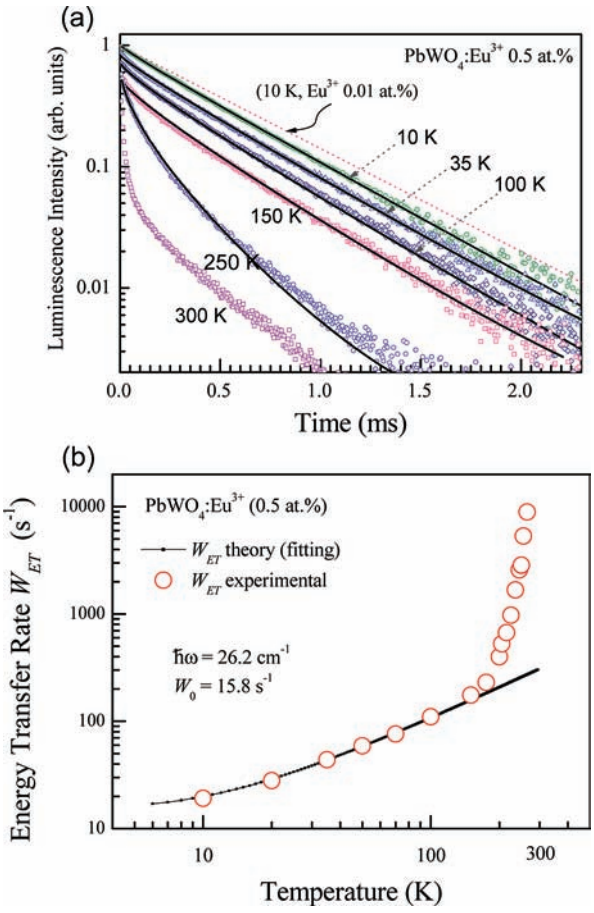

Figure 5. (a) Luminescence decay curves of the $^5D_0$ level for the site E in the $PbWO_4:Eu^{3+}$ (0.5 at.%) crystal at various temperatures. The solid lines are the best fits to the theoretical model in eq 2. The dotted line is the decay curve of $PbWO_4:Eu^{3+}$ (0.01 at.%) at 10 K. (b) The energy-transfer rate W_{ET} at various temperatures obtained by fitting to eq 2. The continuous line represents energy-transfer rate as a function of temperature obtained by fitting to the one-phonon process given in eq 3.

in $PbWO_4:Eu^{3+}$ (0.5 at.%). Comparison of Figures 4a and 5a suggests that for 250 and 300 K (Figure 5a) the decay could consist of two kinds of exponential functions, one of which (initial fast decay for $T > 250$ K in Figure 5a) is due to the same reason as in Figure 4a, that is, energy transfer to killer centers with a characteristic activation energy of 2400 cm^{-1} (Figure 4b). Energy diffusion among Eu^{3+} ions may also contribute to decay, but perhaps it is observable only for longer decay times.

One expects that the energy-transfer rate increases by increasing temperature. The values of energy-transfer rate W_{ET} were obtained at various temperatures by fitting eq 2 and are plotted as a function of temperature in Figure 5b. The temperature-dependent energy-transfer rate in one-phonon process is given by the form[27]

$$W_{ET}(T) = W_{ET}(0)\left[1 - \exp\left(-\frac{\hbar\varpi}{kT}\right)\right]^{-1} \quad (4)$$

where W_{ET} (0) is the energy-transfer rate at 0 K and $\hbar\varpi$ is the average phonon energy needed to bridge the energy gap in a one-phonon process. The W_{ET} (T) is well fitted up to about a temperature of 175 K. The best fit parameters are given in Figure 5b, and the fitting results are summarized in Table 2. However, the temperature dependence of the energy-transfer rate W_{ET} considerably deviates from a one-phonon process at temperatures higher than 175 K. The deviation seems to be due to the highly increased phonon density of states giving rise to the other energy-transfer processes.

TABLE 2: Fitting Results on Critical Energy-Transfer Distance (R_0), Critical Concentration (n_0), Energy-Transfer Rate W_{ET}, and R_0/R_A for $PbWO_4:Eu^{3+}$ (0.5 at.%)

T (K)	R_0 (T), Å	n_0 (T), 10^{20} ions/cm^3	R_0 (T)/R_A	W_{ET} (T), 10^3 s^{-1}
20	8.14	4.41	0.684	0.218
100	8.76	3.55	0.763	0.338
200	9.48	2.80	0.797	0.545
250	12.5	1.08	1.050	2.86

TABLE 3: Number of Eu^{3+} Ions (n) in Unit Volume and Average Distance (R_A) between Nearest-Neighbor Eu^{3+} Ions in $PbWO_4:Eu^{3+}$ (0.01, 0.05, and 0.5 at.%)

$PbWO_4:Eu^{3+}$ (at.%)	n (ions/cm^3) × 10^{20}	R_A (Å)
0.01	0.0283	44.0
0.05	0.1415	24.0
0.5	1.415	11.9

According to Holstein et al.[28,29] and other reports,[30,31] the temperature-dependent energy-transfer rate depends strongly on the particular structure of the electronic energy levels and the site environment in host lattice. For a direct one-phonon process, the energy-transfer rate is proportional linearly to temperature, that is, $W_{ET} \sim T^1$. In two-phonon processes, several energy-transfer processes can be involved in the temperature-dependent phonon-assistant energy-transfer mechanisms, for example, $W_{ET} \sim T^3$ for two-site nonresonant process, $W_{ET} \sim T^7$ (short λ_{phonon}) and $\sim T^9$ (long λ_{phonon}) for one-site Raman process, and $W_{ET} \sim T^7$ for one-site nonresonant processes. The transfer rate between 10 and 175 K in Figure 5b shows approximately T^n ($n = 0.85$) dependence which indicates that one-phonon process is dominant below 175 K in $PbWO_4:Eu^{3+}$ (0.5 at.%). In the temperature region of 175−250 K, the energy-transfer rate is proportional to T^n ($n = 8.3$) which means that the energy transfer is likely to be governed by two-phonon processes between Eu^{3+} ions at higher temperatures in $PbWO_4:Eu^{3+}$ (0.5 at.%). Buijs et al.[30] reported one-phonon-assisted energy transfer at low temperatures and two-phonon two-site nonresonant energy transfer at higher temperatures from the $^5D_0$ level of Eu^{3+} in $Gd_2(MoO_4)_3$ crystals.

The average distance (R_A) between Eu^{3+} ions is calculated to be 44.0, 24.0, and 11.9 Å in $PbWO_4:Eu^{3+}$ (0.01, 0.05, and 0.5 at.%), respectively (see Table 3). The average distance (R_A) is comparable to the critical transfer distance (R_0 (T)) at different temperatures in the $PbWO_4:Eu^{3+}$ crystals. The average distances R_A of 44.0 Å for $PbWO_4:Eu^{3+}$ (0.01 at.%) and 24.0 Å for $PbWO_4:Eu^{3+}$ (0.05 at.%) are sufficiently larger than the transfer distance R_0 (T) of 12.5 Å in $PbWO_4:Eu^{3+}$ (0.5 at.%) at 250 K (see Table 2). This indicates that no energy transfer can take place between Eu^{3+} ions in the $PbWO_4:Eu^{3+}$ (0.01 and 0.05 at.%) crystals at temperature lower than 250 K. On the other hand, the $PbWO_4:Eu^{3+}$ (0.5 at.%) crystal has an R_A of 11.9 Å, which is similar to the critical distance R_0 (T) at the temperature region of 10−300 K (see Table 2). This means that the phonon-assisted energy transfer occurs between Eu^{3+} ions in the $PbWO_4:Eu^{3+}$ (0.5 at.%) crystal even at 10 K. The critical transfer distance R_0 (T) of $PbWO_4:Eu^{3+}$ (0.5 at.%) becomes larger than the average distance R_A of 11.9 Å by increasing temperature over about 210 K.

The decay curves of the $^5D_0$ emission of the minor sites (F, B) and (C, D) in $PbWO_4:Eu^{3+}$ (0.5 at.%) were nearly exponential at 10 K, and the lifetimes were estimated to be about 0.35∼0.40 ms which are shorter than that of site E (0.51 ms). Dependence

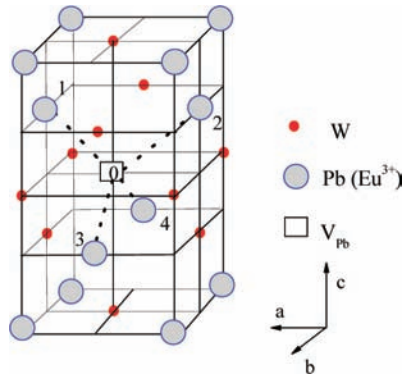

Figure 6. The structural unit cell of $PbWO_4$ crystal.

of lifetime of the minor sites with sample temperature at higher than 100 K could not be investigated because of the weak signal, line broadening, and overlapping with other lines.

4. Distribution of Eu^{3+} Ions in the $PbWO_4$ Lattice. When the Eu^{3+} ions are incorporated in the $PbWO_4$ lattice, Eu^{3+} substitutes for Pb^{2+} and possible charge compensations could be realized in several ways. The excess charge due to the $Eu^{3+} \rightarrow Pb^{2+}$ substitution can be compensated by the formation of Pb^{2+} vacancy or interstitial oxygen O_i^{2-} on two Eu^{3+} ions. The most possible mechanisms of Eu^{3+}-ion doping reactions are known as[9]

$$Eu_2O_3 + PbWO_4 \rightarrow 2Eu_{Pb}^{\bullet} + V_{Pb}'' + 3PbO \quad \text{(i)}$$

$$Eu_2O_3 + PbWO_4 \rightarrow 2Eu_{Pb}^{\bullet} + O_i'' + 2PbO \quad \text{(ii)}$$

The energy calculation confirms that these reactions are possible processes because of lower reaction energies. Equation i has the lowest value,[9] and consequently the first charge compensation by V_{Pb}'' is more favorable. Thus, the dominant excitation line (site E) seems to be corresponding to the $^7F_0 \rightarrow {}^5D_0$ transition of Eu^{3+} associated with the $[2(Eu_{Pb}^{3+})^{\bullet}-V_{Pb}'']$ complex in $PbWO_4:Eu^{3+}$.

The structural unit cell of the $PbWO_4$ crystal is shown in Figure 6. The structure considered is obtained by stacking two unit cells of fluorite type with two types of cations arranged alternately along the *c*-axis in which each Pb^{2+} ion is surrounded by eight O^{2-} ions. In the Scheelite structure, two kinds of combined $Eu_{Pb}^{3+}-V_{Pb}''-Eu_{Pb}^{3+}$ pairs are possible as shown in Figure 6. The one is 1−0−3, 1−0−4, 2−0−3, and 2−0−4 where 0 is V_{Pb} and 1−4 designate the Eu_{Pb}^{3+} ions in closest proximity to V_{Pb}. Another case is 1−0−2 and 3−0−4. The Eu^{3+} ions in two groups of combination have a lower symmetry than S_4, that is, C_1. Taking into account the Coulomb interaction, the former is more stable and, therefore, we except the case of 1−0−2 and 3−0−4 dimers from the possible combinations. The formation of the $[2(M_{pb}^{3+})^{\bullet}-(V_{pb})'']$ complexes by introduction of trivalent cation ions (M^{3+}) into the $PbWO_4$ lattice has been reported.[32,33] Han et al.[32] reported that, in La-doped $PbWO_4$ crystals, the La^{3+} ions are located at the Pb^{2+} sites and combine with lead vacancies to form the dipole complexes $[2(La_{pb}^{3+})^{\bullet}-(V_{pb})'']$ which are the origin of dielectric relaxation process. Lin et al.[34] calculated binding energies of trivalent-ion doping of $PbWO_4$ from which they suggested that trivalent dopants (M^{3+}) generally occupy the Pb^{2+} sites forming the $[(M_{pb}^{3+})^{\bullet}-(V_{pb})'']$ simple pairs and the $[2(M_{pb}^{3+})^{\bullet}-(V_{pb})'']$ dimers and that the oxygen interstitials also coexist in trivalent-ion-doped $PbWO_4$.

It is found in this study, however, no clear evidence of the $x-0-y$ ($x = 1$ or 2 and $y = 3$ or 4) dimers in which the two

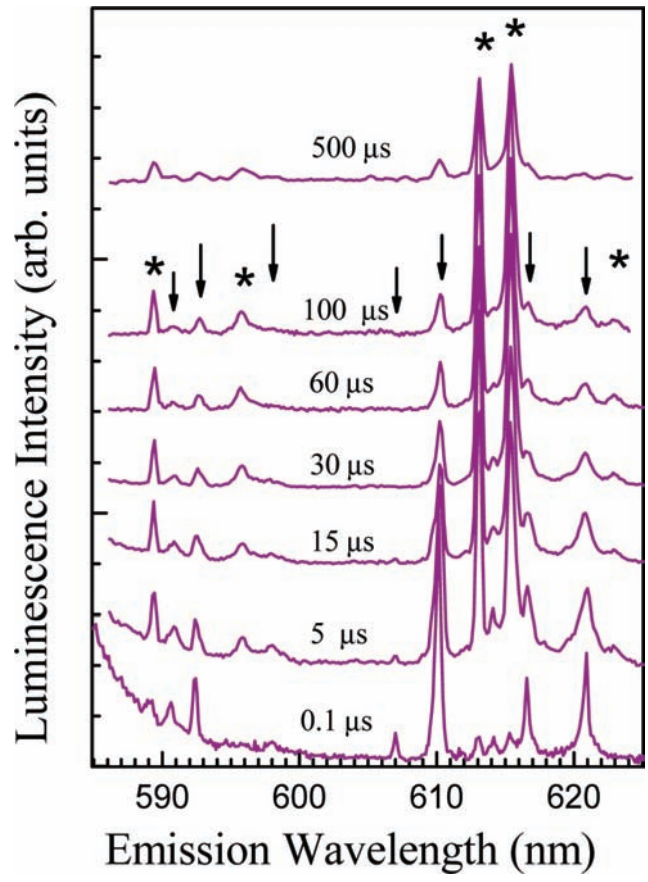

Figure 7. Time-resolved emission spectra of the $^5D_0 \rightarrow {}^7F_J$ ($J = 1$ and 2) transitions exciting into site A (578.06 nm) in $PbWO_4:Eu^{3+}$ (0.5 at.%) at 10 K. The delay times after the laser pulse are denoted. Arrows and asterisks indicate the emission lines representing different temporal behavior (see text).

Eu_{Pb}^{3+} ions are situated at the nearest sides of V_{Pb}. If the Eu_{Pb}^{3+} ions form the $x-0-y$ dimers, energy transfer should take place between two Eu_{Pb}^{3+} ions in the dimer even for low Eu^{3+}-concentration (0.01 at.%) because the distance between Eu_{Pb}^{3+} ions is only 7.15 Å for the $x-0-y$ dimers. However, no energy transfer between Eu^{3+} ions is observed in the $PbWO_4:Eu^{3+}$ (0.01 and 0.05 at.%) crystals in the temperature region of 10−300 K. A large number of Pb^{2+} vacancies (V_{Pb}), oxygen vacancies (V_o), and oxygen interstitials (O_i'') exist in as-grown $PbWO_4$ because of PbO evaporation during the crystal growth, and a variety of intrinsic defects are formed in the $PbWO_4$ lattice.[10−13] When trivalent RE ions are introduced into the $PbWO_4$ crystal, the RE^{3+} ions suppress the defect centers by compensating valence states which may not certainly form the tightly bound $x-0-y$ dimers.

5. Clustering of Eu^{3+} Ions in $PbWO_4:Eu^{3+}$. Figure 7 shows time-resolved emission spectra of the $^5D_0 \rightarrow {}^7F_{1,2}$ transitions obtained by exciting Eu^{3+}(A) at 10 K. The emission spectra consist of two groups of lines belonging to the Eu^{3+}(A) and Eu^{3+}(E) ions (see Figure 7). The lines at 590.8, 592.6, 598.1, 607.0, 610.3, 616.7, and 621.0 nm are assigned for Eu^{3+}(A) (indicated by arrows), and the lines at 589.2, 596.1, 615.0, 616.3, and 623.2 nm are originated to Eu^{3+}(E) (indicated by asterisks). The spectra show apparent time delay characteristic. The emission line changes in relative intensity with different delay times after the laser pulse. The initial intensities of the emission lines from Eu^{3+}(A) are reduced with increasing delay time, while the lines for Eu^{3+}(E) show maximum intensities at around 30 μs with weaker intensities at earlier and later times. When the

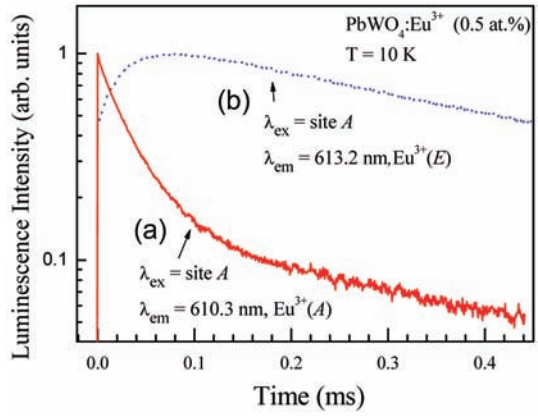

Figure 8. Luminescence decay curves of the selectively monitored $^5D_0$ emissions under the excitation into site A (578.06 nm) in the $PbWO_4:Eu^{3+}$ (0.5 at.%) crystal at 10 K. Curve (a) was obtained by monitoring 610.3 nm emission line (group A(I)). Curve (b) was obtained by monitoring 613.2 nm emission line (group A(II)).

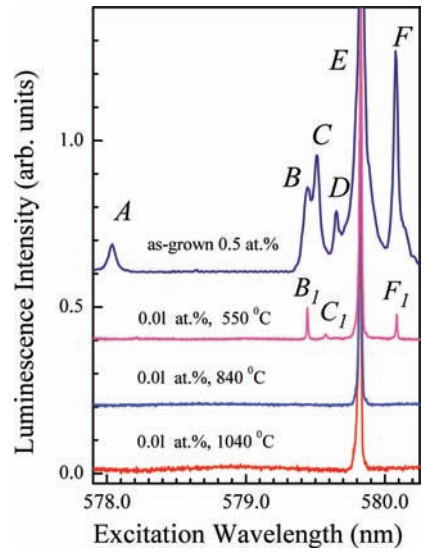

Figure 9. Excitation spectra corresponding to the $^7F_0 \rightarrow {}^5D_0$ transition by monitoring the $^5D_0$ emissions (wavelengths > 581 nm) at 10 K in as-grown $PbWO_4:Eu^{3+}$ (0.5 at.%) and annealed $PbWO_4:Eu^{3+}$ (0.01 at.%) at 550, 840, and 1040 °C in an oxygen atmosphere.

$^5D_0$ level of Eu^{3+} at the other sites (B−F) was excited, we observed no spectral changes in time after the laser pulse.

Figure 8 shows decay curves of each group in Figure 7. The emission lines belonging to Eu^{3+}(A) exhibit a fast decay (30 μs) at the initial stage followed by a long tail with a lifetime of 0.4 ms (Figure 8a), while those belonging to Eu^{3+}(E) show buildup of the emission. The risetime (~35 μs) for the emission from Eu^{3+}(E) (Figure 8b) is similar to the decay time (30 μs) of Eu^{3+}(A) in the initial stage. The decay time of Eu^{3+}(E) after buildup is about 0.50 ms which is similar to the lifetime (0.51 ms) of the emission obtained by directly exciting Eu^{3+}(E). The time-resolved emission spectra (Figure 7) and decay curves (Figure 8) confirm an efficient energy transfer from Eu^{3+}(A) to Eu^{3+}(E).

The spectral and temporal behaviors of Eu^{3+}(A) differ markedly from Eu^{3+} at the other sites (B−F). In comparison with the dominant site E, the excitation line due to the $^7F_0 \rightarrow {}^5D_0$ transition of Eu^{3+}(A) is located at higher energy and the emission has shorter lifetime with nonexponential decay at 10 K. The intensity ratio of the excitation lines A−E was estimated to be 0.019 and 0.10 in $PbWO_4:Eu^{3+}$ (0.05 and 0.5 at.%), respectively, showing that the increase of Eu^{3+} concentration causes significant growth of site A. The luminescence characteristics of Eu^{3+}(A) in $PbWO_4$ are typical for a clustering of Eu^{3+} ions in a host lattice. It is reported that clustering of RE^{3+} ions takes place in addition to isolated RE^{3+} ions with vacancies or any other defects.[14,35] The binding energies of the nearest neighbor (nn), the next nearest neighbor (nnn), and the next next nearest neighbor (nnnn) configurations have negative values in $PbWO_4$.[9] The dopant ions, therefore, can have a tendency to bind together to form Eu^{3+}-clusters in $PbWO_4$. Nikl et al.[36] reported that for heavily doped samples in La^{3+} doped $PbWO_4$, doping with La^{3+} of several hundred molar ppm in the crystal could create new centers at which efficient nonradiative recombination of free carriers takes place in these killer sites because of La^{3+} aggregates in the $PbWO_4$ structure. Similar effects can also exert on clustered Eu^{3+} in $PbWO_4$ leading to strong changes in the spectral feature and temporal behavior in comparison with the isolated Eu^{3+} ions at the other sites in $PbWO_4:Eu^{3+}$.

6. Annealing Effects. The oxygen defects, for example, interstitial oxygen O_i and oxygen vacancy V_O, which can be formed and changed during the annealing treatment in air atmosphere, have strong influence on structural disorder and luminescence in $PbWO_4$;[11,37] Figure 9 shows the excitation spectra of the $^7F_0 \rightarrow {}^5D_0$ transition in annealed $PbWO_4:Eu^{3+}$ (0.01 at.%) in oxygen atmosphere at 550, 840, and 1040 °C. In comparison with as-grown $PbWO_4:Eu^{3+}$ (0.01 at.%) (Figure 1), new excitation lines appear for the annealed $PbWO_4:Eu^{3+}$ (0.01 at.%) at 550 °C**.** The new peaks are labeled by B_1 (579.50 nm), C_1 (579.54 nm), and F_1 (580.08 nm). The excitation lines B_1 and F_1 appear at the same wavelengths as the excitation lines for sites B and F in $PbWO_4:Eu^{3+}$ (0.05 and 0.5 at.%), while the excitation line C_1 is a little bit shifted from the excitation line C. These new peaks completely disappear by further annealing of $PbWO_4:Eu^{3+}$ (0.01 at.%) at 840 and 1040 °C (Figure 9). It has been well established that most changes in the $PbWO_4$ lattice are oxygen components during annealing at different temperatures.[11] The result in Figure 9 clearly shows that the annealing gives rise to interstitial oxygen coupled with Eu^{3+} in $PbWO_4:Eu^{3+}$ (0.01 at.%) lattices.

The emission spectra and decay curves were obtained by exciting the E, B_1, and F_1 centers in annealed $PbWO_4:Eu^{3+}$(0.01 at.%) and were found to have nearly the same spectral feature and temporal behavior as those of sites E, B, and F of as-grown $PbWO_4:Eu^{3+}$(0.5 at.%), respectively. This supports that the origin of Eu^{3+}(F) and Eu^{3+}(B) in $PbWO_4:Eu^{3+}$ (0.05 and 0.5 at.%) is similar to $Eu^{3+}(F_1)$ and $Eu^{3+}(B_1)$ in annealed $PbWO_4:Eu^{3+}$ (0.01 at.%) at 550 °C, respectively. However, the origin of Eu^{3+}(C) in $PbWO_4:Eu^{3+}$ (0.05 and 0.5 at.%) is certainly different from that of $Eu^{3+}(C_1)$ in annealed $PbWO_4:Eu^{3+}$ (0.01 at.%). The excitation line C_1 was not detected in $PbWO_4:Eu^{3+}$ (0.05 and 0.5 at.%) because it may be too weak to be observed and probably overlapped with other lines.

According to the annealing mechanism for $PbWO_4:Gd^{3+}$ and pure $PbWO_4$,[37,38] the following process of creation of O_i and the transformation of charge association could take place:

$$PWO + 1/2O_2 \rightarrow O_i'' + 2h \quad \text{(iii)}$$

$$[2(Eu_{Pb}{}^{3+})^{\bullet} - V_{Pb}''] + O_O{}^{\times} \rightarrow [2(Eu_{Pb}{}^{3+})^{\bullet} - (O_i{}^{2-})''] + [V_{Pb} - V_O] \quad \text{(iv)}$$

The reaction temperature (550 °C) of process iv for $PbWO_4$:Eu^{3+} (0.01 at.%) is lower than that of pure $PbWO_4$ (640 °C) [ref 37] which is likely to be due to the disturbance of doped Eu^{3+} ions. At higher annealing temperatures between 840 and 1040 °C, there exists the following process:

$$O_i'' + 2h^{\bullet} \rightarrow 1/2O_2(\text{ad.}) \rightarrow 1/2O_2(\text{gas}) \quad \text{(v)}$$

As a result, O_i diffuses out of the $PbWO_4$ lattice. Disappearance of O_i should be correlated with the vanishing of excitation peaks B_1, C_1, and F_1 (Figure 9).

When RE^{3+} concentration is raised, more Pb vacancies (V_{Pb}) are formed in the $PbWO_4$ lattice, which might exceed the ability to accommodate for the Scheelite structure $PbWO_4$ crystal.[39] However, $PbWO_4$ keeps the Scheelite structure well even after heavily doping, for example, doping of La^{3+} ion by 15 mol % in $PbWO_4$ crystal[34] and $Pb_{0.7}La_{0.3}WO_{4.15}$ ceramics.[40] To keep the Scheelite structure, another charge balance should appear by O_i[41] as shown in eq ii. $Eu_{Pb}{}^{3+}$ associated with O_i in eq ii is similar to that in eq iv indicating that sites B and F in $PbWO_4$:Eu^{3+} (0.05 and 0.5 at.%) have an origin similar to sites B_1 and F_1 in annealed $PbWO_4$:Eu^{3+} (0.01 at.%), respectively. The emission spectrum of Eu^{3+}(C) is rather close to the spectrum of Eu^{3+}(E) as shown in Figure 3. Therefore, the excitation line C comes probably from Eu^{3+} at the sites perturbed by site E.

IV. Conclusion

We identify six different Eu^{3+} centers in the $PbWO_4$:Eu^{3+} crystals by site-selective laser-excitation spectroscopy. For low concentration (0.01 at.%) of Eu^{3+}, only the dominant Eu^{3+} center with the $^5D_0$ level at 578.95 nm (site E) is observed. The five minor sites A, B, C, D, and F appear together with the dominant site E in high Eu^{3+} concentration (0.05 and 0.5 at.%). The relative emission intensities of the five minor sites to site E are increased by increasing concentration. Eu^{3+} at site E originates from $[2(Eu_{Pb}{}^{3+})^{\bullet} - (V_{Pb})'']$ formed by charge compensation. New sites B_1 and F_1 in annealed $PbWO_4$:Eu^{3+}(0.01 at.%) at 550 °C are associated with interstitial oxygen O_i corresponding to sites B and F, respectively, in as-grown $PbWO_4$:Eu^{3+} (0.05 and 0.5 at.%). Sites C and D are attributed to the sites perturbed by dominant site E. A clustering of Eu^{3+} ions forming site A occurs at high concentration of Eu^{3+} (0.05 and 0.5 at.%). From the dependence of lifetime with temperature, we conclude that thermal quenching occurs from Eu^{3+} to killer centers (defect centers) in $PbWO_4$:Eu^{3+} (0.01 and 0.05 at.%) in temperature higher than 175 K. Energy transfer occurs between the isolated Eu^{3+} ions (mostly the ions at site E) in $PbWO_4$:Eu^{3+} (0.5 at.%) even at 10 K. Energy diffusion takes place together with thermal quenching at temperature higher than 175 K.

Acknowledgment. This work was supported by the Korea Research Foundation Grant funded by the Korean Government (MOEHRD, Basic Research Promotion Fund) (KRF - 2007 - 313 - C00312).

References and Notes

(1) Kobayashi, M.; Usuki, Y.; Ishii, M.; Yazawa, T.; Hara, K.; Tanaka, M.; Nikl, M.; Nitsch, K. *Nucl. Instrum. Methods Phys. Res., Sect. A* **1997**, *399*, 261.
(2) Nikl, M. *Phys. Status Solidi A* **2000**, *178*, 595.
(3) Kobayshi, M.; Sugimoto, S.; Yoshimura, Y.; Komatsubara, T. K.; Mimori, K.; Omata, K.; Ekiguchi, S. T.; Fujiwara, T.; Usuki, Y.; Ishii, M. *Nucl. Instrum. Methods Phys. Res., Sect. A* **2002**, *484*, 140.
(4) Chen, W.; Inagawa, Y.; Tateda, M.; Takeuchi, N.; Usuki, Y. *Opt. Commun.* **2001**, *194*, 401.
(5) Kaminskii, A. A.; Eichler, H. J.; Ueda, K.; Klassen, N. V.; Redkin, B. S.; Li, L. E.; Findeisen, J. F.; Jaquem, D.; Garcia-soli, J.; Fernandez, J.; Balda, R. *Appl. Opt.* **1999**, *38*, 4538.
(6) Kobayashi, M.; Sugimoto, S.; Yoshimura, Y.; Usuki, Y.; Ishii, M.; Senguttuvan, N.; Tanji, K.; Nikl, M. *Nucl. Instrum. Methods Phys. Res., Sect. A* **2001**, *459*, 482.
(7) Esaka, T. *Solid State Ionics* **2000**, *136−137*, 1.
(8) Li, W.; Feng, X.; Huang, Y. *J. Phys.: Condens. Matter* **2004**, *16*, 1325.
(9) Lin, Q.; Feng, X. *J. Phys.: Condens. Matter* **2003**, *15*, 1963.
(10) Lin, Q.; Feng, X.; Man, Z. *Phys. Rev. B* **2001**, *63*, 134105.
(11) Laguta, V. V.; Martini, M.; Vedda, A.; Rosetta, E.; Nikl, M.; Mihóková, E.; Rosa, J.; Usuki, Y. *Phys. Rev. B* **2003**, *67*, 205102.
(12) Abraham, Y. B.; Holzwarth, N. A. W.; Williams, R. T.; Matthews, G. E.; Tackett, A. R. *Phys. Rev. B* **2001**, *64*, 245109.
(13) Laguta, V. V.; Martini, M.; Vedda, A.; Nikl, M.; Mihokova, E.; Bohacek, P.; Rosa, J.; Hofstatter, A.; Meyer, B. K.; Usuki, Y. *Phys. Rev. B* **2001**, *64*, 165102.
(14) Seo, H. J.; Tsuboi, T.; Jang, K. *Phys. Rev. B* **2004**, *70*, 205113.
(15) Zhang, W.; Seo, H. J.; Moon, B. K.; Yi, S.; Jang, K. *J. Alloys Compd.* **2004**, *374*, 32.
(16) Xiong, F.; Lin, Y.; Chen, Y.; Luo, Z.; Ma, E.; Huang, Y. *Chem. Phys. Lett.* **2006**, *429*, 410.
(17) Mirova, I. S.; Fedorova, V. V.; Moskaleva, I. S.; Martyshkina, D. V.; Beloglovskic, S. Y.; Burachasc, S. F.; Savelievc, Y. A.; Tseitlinec, A. M. *Opt. Mater.* **2008**, *31*, 94.
(18) Chen, Y.; Lin, Y.; Luo, Z.; Huang, Y. *J. Opt. Soc. Am. B* **2005**, *22*, 898.
(19) Huang, Y.; Tsuboi, T.; Seo, H. J. *J. Phys. Chem. A* **2008**, *112*, 5839.
(20) Sattler, J. P.; Nemarich, J. *Phys. Rev. B* **1970**, *1*, 4249.
(21) Görller-Walrand, C.; Binnemans, K. Rationalization of Crystal-Field Parametrization. In *Handbook on the Physics and Chemistry of Rare Earths*; Gschneidner, K. A., Jr., Eyring, L., Eds.; North-Holland: Amsterdam, 1996; Vol. 23, p 155.
(22) Wang, J.; Righini, M.; Gnoli, A.; Foss, S.; Finstad, T.; Serincan, U.; Turan, R. *Solid State Commun.* **2008**, *147*, 461.
(23) Wang, J.; Song, H.; Kong, X.; Xu, W.; Xia, H. *J. Appl. Phys.* **2002**, *91*, 9466.
(24) Inokuti, M.; Hirayama, F. *J. Chem. Phys.* **1965**, *43*, 1978.
(25) Wright, J. C. Up-conversion and Excited State Energy Transfer in Rare-Earth Doped Materials. In *Topics in Applied Physics*; Fong, F. K., Ed.; Springer: Berlin, 1976; Vol. 15, p 239.
(26) Henderson, B.; Imbusch, G. F. *Optical Spectroscopy of Inorganic Solids*; Clarendon Press: Oxford, U.K., 1989; p 453.
(27) Hüfner, S. *Optical Spectra of Transparent Rare Earth Compounds*; Academic Press: New York, 1978; p 140.
(28) Holstein, T.; Lyo, S. K.; Orbach, R. *Phys. Rev. Lett.* **1977**, *36*, 891.
(29) Holstein, T.; Lyo, S. K.; Orbach, R. In *Laser Spectroscopy of Solids*; Yen, W. M., Selzer, P. M., Eds.; Springer: Berlin, 1981; Chapter 2.
(30) Buijs, M.; Blasse, G.; Brixner, L. H. *Phys. Rev. B* **1986**, *34*, 8815.
(31) Chen, X. Y.; Zhao, W.; Cook, R. E.; Liu, G. K. *Phys. Rev. B* **2004**, *70*, 205122.
(32) Han, B. G.; Feng, X. Q.; Hu, G. Q.; Wang, P. C.; Yin, Z. W. *J. Appl. Phys.* **1998**, *84*, 2831.
(33) Li, W. S.; Tang, T. B.; Huang, H. W.; Feng, X. Q. *Jpn. J. Appl. Phys* **2001**, *40*, 6893.
(34) Lin, Q. S.; Feng, X. Q.; Man, Z. Y.; Qi, Z. M.; Shi, C. S. *Chin. J. Struct. Chem* **2001**, *20*, 214.
(35) Ramponi, A. J.; Wright, J. C. *Phys. Rev. B* **1987**, *35*, 2413.
(36) Nikl, M.; Bohacek, P.; Nitsch, K.; Mihokova, E. *Appl. Phys. Lett.* **1997**, *71*, 3755.
(37) Huang, Y.; Wen, L. Z.; Feng, X. *J. Electron Spectrosc.* **2003**, *133*, 39.
(38) Huang, H. W.; Ye, Z. G.; Dong, M.; Zhu, W. L.; Feng, X. Q. *Jpn. J. Appl. Phys.* **2002**, *41*, 713.
(39) Linn, S. A. W.; Olefin, W. J. *Ann. N.Y. Acad. Sci.* **1976**, *272*, 22.
(40) Esaka, T.; Mina-ai, T.; Iwahara, H. *Solid State Ionics* **1992**, *57*, 319.
(41) Zhu, W. L.; Feng, X. Q.; Huang, Y. L.; Lin, Q. S.; Wu, Z. H. *Phys. Status Solidi A* **2002**, *193*, 211.

JP901099H